

Generation of Large Kitten states via thermally driven dissipative freezing

Caspar Groiseau^{1,2,*}

¹*Departamento de Física Teórica de la Materia Condensada and Condensed Matter Physics Center (IFIMAC),
Universidad Autónoma de Madrid, 28049 Madrid, Spain*

²*Department of Microtechnology and Nanoscience (MC2),
Chalmers University of Technology, SE-412 96 Gothenburg, Sweden*

(Dated: September 3, 2025)

We show that one can exploit the representation of the Dicke state with magnetic quantum number 0 in orthogonal bases to increase the probability of producing a large Kitten state or even a Cat state via dissipative one-axis twisting, resulting in a net increase in metrological sensitivity and robustness against white noise with respect to the initial state. The resulting states are also useful for quantum secret sharing. The success of the scheme is heralded by the rate of photoemissions. Unlike previous iterations, we have an important population of the larger Kitten states, which makes post-selecting trajectories for them feasible.

Keywords: Quantum Optics, Quantum State Engineering, Dicke model

I. INTRODUCTION

A Cat state, named in analogy to Schrödinger's thought experiment [1], is a superposition of two quasi-classical states. They are susceptible even to small perturbations, as can be seen by their high frequency interference patterns in the Wigner function. This makes them excellent for quantum-enhanced measurements and important for the field of quantum metrology [2]. The generalized Greenberger-Horne-Zeilinger (GHZ) state is a specific type of Cat state important in the context of quantum secret sharing [3].

Cat states have been realized in a great variety of systems ranging from optical photons [4, 5], single Rydberg atoms [6], cold atoms [7], microwave photons with superconducting circuits [8], trapped ions [9] and SQUIDS [10]. The Cat states based on the superposition of photonic states are relatively fragile [11, 12]. In that regard, the angular momentum degree of freedom of matter seems to be more promising in producing large Cat states. However, in spinor systems the time scales can be slow due to weak interaction between particles. Recent initiatives have addressed this by implementing effective Dicke models, known for their strong cavity-mediated collective interactions. This has been achieved in atoms [13], trapped ions [14, 15] and BECs [16, 17].

Decoherence or dissipation, stemming from quantum systems being open and in constant interaction with an environment, represents one of the largest obstacles in modern quantum physics, as it typically destroys the coherences that make quantum dynamics so advantageous. It can, however, also be a constructive effect in certain circumstances, e.g., when trying to generate a quantum state that is a dark or steady state. Proposals to exploit dissipation include dissipative quantum computation [18], stabilization of topological edge states [19], improvement of the purity and phase coherence of BECs [20], and preparation of entangled [21–23] and spin-squeezed states [24].

We build on the work in [25–27], in which it was observed that a symmetric superposition of the eigenstates of the Liouvillian evolving under "dissipative one-axis twisting" will settle (or freeze) in an entangled-state cycle. These entangled-state cycles consisted of pairs of Kitten states (Cat state with smaller magnetic quantum number $|S, \pm m\rangle, m < S$), between which the system indefinitely alternates via photoemissions. However, the likelihood of these cycles was determined by the initial population of the corresponding Dicke states. In [25, 26] a spin-coherent state (in a basis orthogonal to the twisting axis) and in [27] an equal superposition of all eigenstates were considered. The former had vanishing population of the large Kitten states and for the latter, it is unclear how to obtain it. Here we make use of the fact that the non-spin-coherent Dicke states, which can be experimentally achieved, have also representation as symmetric superpositions in orthogonal bases and show this can massively improve the likelihood of obtaining a large Kitten state. This is exemplified here for the optimal choice $|S, 0\rangle$. FIG. 1 shows the Wigner functions of this initial state and of resulting large and small Kitten states.

The paper is organized as follows: first, we present how to get from the Dicke model to the required dissipative one-axis twisting dynamics. Then, we show how the Dicke state $|S, 0\rangle_x$ evolves under these dynamics and show how this can result in large Kitten states. Then we explore the potential usefulness of these states in quantum secret sharing and quantum metrology. Following that, we discuss the experimental feasibility, specifically the generation of the initial state and the influence of single-particle decoherence. Finally, we make our closing remarks and provide an outlook.

II. MODEL

We consider a system of N identical spinors with total integer spin S interacting with a cavity mode \hat{a} in a Dicke model. The master equation for the density

* groiseau@chalmers.se

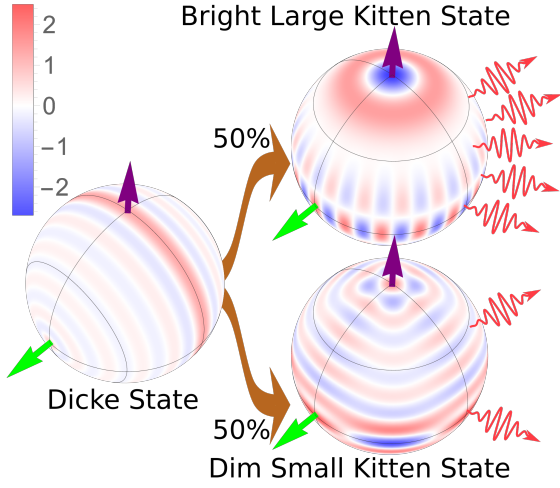


FIG. 1. Schematic representation of the idea: the Dicke state $|S = 10, m = 0\rangle_x$ is transformed into either a large or a small Kitten state with equal probability. We display here the Wigner functions [2, 28] of a large Kitten state exemplified by $(|S = 10, m = 9\rangle_y + |S = 10, m = -9\rangle_y)/\sqrt{2}$ and a small Kitten state exemplified by $(|S = 10, m = 2\rangle_y + |S = 10, m = -2\rangle_y)/\sqrt{2}$. The green arrow points in x -direction and the purple arrow in y -direction.

operator $\hat{\rho}$ for this configuration is given by ($\hbar = 1$)

$$\dot{\hat{\rho}} = -i \left[\hat{H}_{\text{Dicke}}, \hat{\rho} \right] + \kappa(\mathbf{n} + 1) \mathcal{D}[\hat{a}] \hat{\rho} + \kappa \mathbf{n} \mathcal{D}[\hat{a}^\dagger] \hat{\rho}, \quad (1)$$

where we account for a thermal population of the cavity \mathbf{n} . We define the Lindblad superoperator $\mathcal{D}[\hat{O}] \hat{\rho} = 2\hat{O} \hat{\rho} \hat{O}^\dagger - \hat{\rho} \hat{O}^\dagger \hat{O} - \hat{O}^\dagger \hat{O} \hat{\rho}$ [29]. The Hamiltonian of the Dicke model is given by

$$\begin{aligned} \hat{H}_{\text{Dicke}} = & \omega \hat{a}^\dagger \hat{a} + \omega_0 \hat{S}_z + \frac{\lambda_-}{\sqrt{2S}} \left(\hat{a} \hat{S}_+ + \hat{a}^\dagger \hat{S}_- \right) \\ & + \frac{\lambda_+}{\sqrt{2S}} \left(\hat{a} \hat{S}_- + \hat{a}^\dagger \hat{S}_+ \right), \end{aligned} \quad (2)$$

expressed it in terms of collective spin operators $\hat{S}_{\{x,y,z,\pm\}} = \sum_n \hat{S}_{\{x,y,z,\pm\}}^{(n)}$, where $\hat{S}_{\{x,y,z,\pm\}}^{(n)}$ are the spin operators of the n -th spinor.

In the limit $\sqrt{\omega^2 + \kappa^2} \gg \omega_0, \lambda_\pm$, the cavity can be adiabatically eliminated to obtain [30]

$$\begin{aligned} \dot{\hat{\rho}} = & -i \left[\hat{H}, \hat{\rho} \right] + \frac{\kappa(\mathbf{n} + 1)}{2S(\omega^2 + \kappa^2)} \mathcal{D}[\lambda_- \hat{S}_- + \lambda_+ \hat{S}_+] \hat{\rho} \\ & + \frac{\kappa \mathbf{n}}{2S(\omega^2 + \kappa^2)} \mathcal{D}[\lambda_- \hat{S}_+ + \lambda_+ \hat{S}_-] \hat{\rho}, \end{aligned} \quad (3)$$

with the Hamiltonian

$$\begin{aligned} \hat{H} = & \left[\omega_0 - \frac{\omega(2\mathbf{n} + 1)(\lambda_-^2 - \lambda_+^2)}{2S(\omega^2 + \kappa^2)} \right] \hat{S}_z \\ & - \frac{\omega}{2S(\omega^2 + \kappa^2)} \left[(\lambda_- + \lambda_+)^2 \hat{S}_x^2 + (\lambda_- - \lambda_+)^2 \hat{S}_y^2 \right]. \end{aligned} \quad (4)$$

We are considering a scheme, completely dissipative in nature, in particular, we will be setting $\omega = \omega_0 = 0$ in Eqs. (3-4). Additionally, we set $\lambda_+ = -\lambda_- = -\lambda$. Both these changes can be achieved by tuning

the frequency, strengths and phases of the driving and cavity fields [26, 30, 31]. We end up with the master equation

$$\dot{\hat{\rho}} = \Upsilon \mathcal{D}[\hat{S}_y] \hat{\rho}, \quad (5)$$

where $\Upsilon = 2\lambda^2(2\mathbf{n} + 1)/(S\kappa)$.

III. DISSIPATIVE FREEZING AND ENTANGLED-STATE CYCLES

Let us assume that our initial state is the Dicke state with magnetic quantum number $m = 0$ in the x -basis (denoted by the subscript on the ket)

$$|\psi(t = 0)\rangle = |S, 0\rangle_x. \quad (6)$$

Since the evolution in Eq. (5) depends only on \hat{S}_y , a change of basis from the eigenstates of \hat{S}_x to those of \hat{S}_y is in order. To this end we can use

$$|S, m'\rangle_x = \sum_{m=-S}^S d_{m,m'}^S \left(-\frac{\pi}{2} \right) |S, m\rangle_y, \quad (7)$$

where $d_{m,m'}^S(\beta) = {}_z\langle S, m | e^{-i\beta \hat{S}_y} | S, m' \rangle_z$ are the elements of the Wigner d matrix [32]. In the special case where $m' = 0$, we can represent it in terms of the spherical harmonics $Y_S^m(\theta, \varphi)$, i.e.,

$$d_{m,0}^S = \sqrt{\frac{4\pi}{2S+1}} Y_S^m \left(-\frac{\pi}{2}, 0 \right). \quad (8)$$

Note that if S is even/odd, then only the even/odd Dicke states $|S, m\rangle_y$ have non-zero amplitudes $d_{m,0}^S$ and we have $d_{-m,0}^S = (-1)^S d_{m,0}^S$.

We unravel the Master equation to describe the evolution of a single quantum trajectory [33]. Each time step Δt , we evolve the wave function with the non-Hermitian Hamiltonian $\hat{H}_{NH} = -i\Upsilon \hat{S}_y^2$. This comes with a loss proportional to the probability of a quantum jump, i.e., $\Delta t \langle \psi(t) | 2\Upsilon \hat{S}_y^2 | \psi(t) \rangle$. We determine whether a jump happened with a random number generator and if so apply \hat{S}_y to the wave function. In both cases, we renormalize the wave function afterwards. With this we can rewrite the wave function between jumps with Eq. (5) as

$$\begin{aligned} |\psi(t)\rangle = & \frac{e^{-\Upsilon \hat{S}_y^2 t} |\psi(0)\rangle}{\|e^{-\Upsilon \hat{S}_y^2 t} |\psi(0)\rangle\|} = \frac{\sum_m d_{m,0}^S e^{-\Upsilon m^2 t} |S, m\rangle_y}{\sqrt{\sum_m e^{-2\Upsilon m^2 t} (d_{m,0}^S)^2}} \\ = & \frac{d_{0,0}^S |S, 0\rangle_y + \sum_{m=1}^S d_{m,0}^S e^{-\Upsilon m^2 t} \sqrt{2} |\chi_S^+(m)\rangle}{\sqrt{\sum_m e^{-2\Upsilon m^2 t} (d_{m,0}^S)^2}}, \end{aligned} \quad (9)$$

where $|\chi_S^\pm(m)\rangle$ are the Kitten states

$$|\chi_S^\pm(m)\rangle = \frac{1}{\sqrt{2}} (|S, m\rangle_y \pm (-1)^S |S, -m\rangle_y). \quad (10)$$

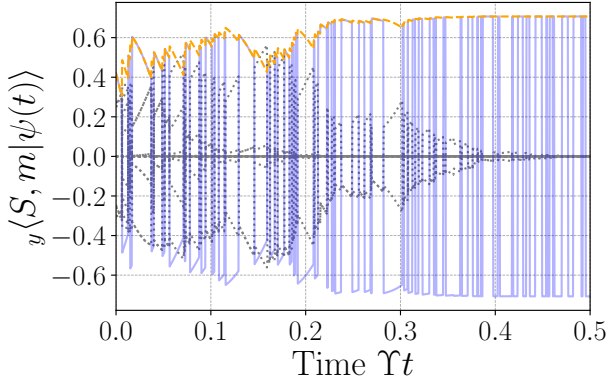


FIG. 2. Single-trajectory simulation of the overlap of the system state with the eigenstates of \hat{S}_y . We plot the overlap with the two Dicke states $\langle\psi(t)|S, -m\rangle_y$ (solid blue) and $\langle\psi(t)|S, m\rangle_x$ (dashed orange) for the m -value that corresponds to the final, surviving entangled-state cycle, and the overlaps remaining Dicke states (dotted grey) as a function of time for a single trajectory of spin $S = 10$. The trajectory shows a cycle that settles in the Cat state $m = S$.

After the first jump (photoemission), the $|S, 0\rangle_y$ -component of $|\psi(t)\rangle$ is eliminated. Since all $|S, m \neq 0\rangle_y$ decay, the system emits photons ad infinitum. FIG. 2 shows how in the limit of large time t only one pair $|\chi_S^\pm(m)\rangle$ survives, due to the positive feedback loop between the rate of photoemissions and the populations of $|S, m\rangle_y$ (cf. [25, 26]). This can also be understood by \hat{S}_y being a strong symmetry of the system (commuting with the Hamiltonian and the Lindblad operator) [27]. The probability for a specific entangled-state cycle to occur $P_{|\chi_S(m)\rangle} = 2(d_{S,0}^S)^2$ (without the factor 2 if $m = 0$) is tantamount to the initial population $|\langle S, 0|\chi_S^\pm(S)\rangle|^2$ because Dicke states $|S, m\rangle_y$ are steady states of Eq. (5) in the trajectory average. In [34] ideas to steer lower entangled-state cycles into higher ones were explored, but remained mostly hypothetical. Each jump also changes the relative sign within the Kitten states since

$$\hat{S}_y |\chi_S^\pm(m)\rangle = m |\chi_S^\mp(m)\rangle, \quad (11)$$

so that the system switches back and forth between the two states $|\chi_S^\pm(m)\rangle$ (vertical lines in FIG. 2). The rate at which it does this allows us to determine in what cycle the system has settled in, because the rate scales quadratically with m , i.e.,

$$\langle\chi_S^\pm(m)|\hat{S}_y^2|\chi_S^\pm(m)\rangle = m^2. \quad (12)$$

The rate could be determined by performing a photon counting measurement on the cavity output. As highlighted in [25], conducting a homodyne measurement on the cavity output instead of photon counting and thereby determining $\langle m \rangle$ instead of $\langle m^2 \rangle$, could be used to force the system to settle into the corresponding Dicke state.

FIG. 3 shows a histogram of the probability of ending in the entangled-state cycle $|\chi_S^\pm(m)\rangle$. The initial state $|S, 0\rangle_x$ offers a distribution that is significantly skewed towards larger m , and is therefore much

more likely to produce large Kitten states than a spin-coherent state [25, 26] or a uniform distribution [27]. In fact the Cat states $|\chi_S^\pm(S)\rangle$ are the most likely outcome with probability

$$P_{\text{Cat}} = 2(d_{S,0}^S)^2 = 2 \frac{(2S)!}{2^{2S}(S!)^2} \approx \frac{2}{\sqrt{\pi S}}, \quad (13)$$

which is a factor $\exp(S)$ larger than if we had started with a spin-coherent state [25, 26]. Here we used that $Y_S^{\pm S}(\theta, 0) = (\mp 1)^S \sqrt{(2S+1)!/(4\pi)} \sin^S \theta / (2^S S!)$ and Stirling's formula ($S! \approx S^S e^{-S} \sqrt{2\pi S}$).

IV. POTENTIAL APPLICATIONS

A. Quantum Secret Sharing

In quantum secret sharing, the goal is that sender Alice A shares a secret with a number of other parties called Bob B so that only together all Bobs can access the secret [3]. The Kitten states in the standard basis representation ($N = 2S$ spin 1/2-spinors) are given by

$$|\chi_S^\pm(m)\rangle = \frac{\sum (|1^{\otimes S+m} 0^{\otimes S-m}\rangle_y \pm |1^{\otimes S-m} 0^{\otimes S+m}\rangle_y)}{\sqrt{2 \binom{2S}{S-m}}}, \quad (14)$$

where we sum all permutations. The crucial property for quantum secret sharing is that

$$\begin{aligned} \langle\chi_S^\pm(m)|\hat{\sigma}_z^{2S}|\chi_S^\pm(m)\rangle &= \pm 1, \\ \langle\chi_S^\pm(m)|\hat{\sigma}_z^{2S}|\chi_S^\mp(m)\rangle &= \pm (-1)^{S+m}. \end{aligned} \quad (15)$$

This allows the $2S - 1$ Bobs if and only if they perform the same measurement with the results R_{B_i} and

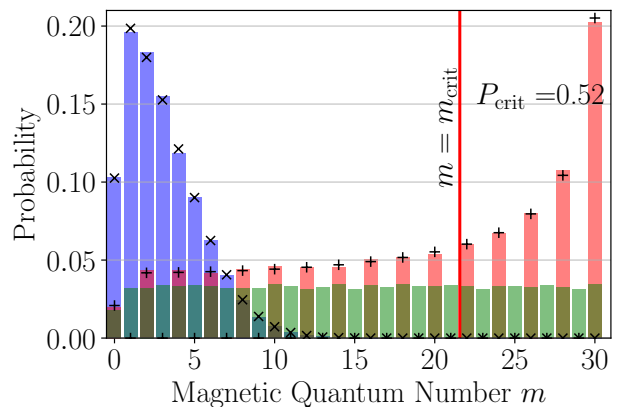


FIG. 3. Histogram of the probability to land in each entangled-state cycle for the initial state $|S, S\rangle_x$ (blue) equal distribution of all $|S, 0\rangle_y$ (green) and $|S, 0\rangle_x$ (red), for $S = 30$ and averaged over 50000 quantum trajectories. The vertical line represent the value of m_{crit} , left of which lies the highlighted are that represents the entangled-cycles with increased QFI compared to $|S, 0\rangle_x$ (with total probability P_{crit}). The black pluses and crosses represent the analytical values for the initial populations $|\langle S, 0|\chi_S^\pm(S)\rangle|^2$ and $|\langle S, S|\chi_S^\pm(S)\rangle|^2$, respectively.

cooperate to deduce the result of Alice's measurement result R_A via $R_A = \langle \hat{\sigma}_{z,x}^{2S} \rangle / (R_{B_1} \dots R_{B_{2S-1}})$. As soon as one Bob is taken out of this process, Alice's result is left secret. The scheme does require exact knowledge of the initial state, which would require keeping track of the number of photodetections during the generation of the Kitten state.

An eavesdropper Evan with an associated ancillary qubit E might spoil the secret. We have

$$|\chi_S^\pm(m)\rangle = \frac{1}{\sqrt{2}}(|0\rangle_A |\xi\rangle_B \pm |1\rangle_A |\bar{\xi}\rangle_B), \quad (16)$$

where

$$\begin{aligned} |\xi\rangle &= \frac{\sum (|1^{\otimes S+m} 0^{\otimes S-m-1}\rangle_y \pm |1^{\otimes S-m} 0^{\otimes S+m-1}\rangle_y)}{\sqrt{2^{\binom{2S}{S-m}}}} \\ |\bar{\xi}\rangle &= \frac{\sum (|1^{\otimes S+m-1} 0^{\otimes S-m}\rangle_y \pm |1^{\otimes S-m-1} 0^{\otimes S+m}\rangle_y)}{\sqrt{2^{\binom{2S}{S-m}}}}, \end{aligned} \quad (17)$$

where the \pm relates to $|\chi_S^\pm(m)\rangle$. The optimal coherent individual attack tries to establish entanglement between Alice and Evan via

$$\begin{aligned} \hat{U}_{BE} |\xi\rangle_B |0\rangle_E &= |\xi\rangle_B |0\rangle_E \\ \hat{U}_{BE} |\bar{\xi}\rangle_B |0\rangle_E &= \cos \phi |\bar{\xi}\rangle_B |0\rangle_E + \sin \phi |\xi\rangle_B |1\rangle_E, \end{aligned} \quad (18)$$

where $\phi \in [0, \pi/2)$ corresponds to the strength of the attack. This leaves the system in the quantum state

$$\begin{aligned} \hat{U}_{BE} |\chi_S^\pm(m)\rangle |0\rangle_E &= \frac{1}{\sqrt{2}}(|0\rangle_A |\xi\rangle_B |0\rangle_E \\ &+ \cos \phi |1\rangle_A |\bar{\xi}\rangle_B |0\rangle_E + \sin \phi |1\rangle_A |\xi\rangle_B |1\rangle_E), \end{aligned} \quad (19)$$

which takes the same form as for a G -state ($|\chi_S^\pm(S-1)\rangle$). This was shown to be secure in the regime $\phi \in [0, \pi/4)$, i.e. the two-qubit Bell inequality is violated between Alice and any of the Bobs and not between Alice and Evan [35].

B. Quantum Metrology

The sensitivity of a pure state $|\psi\rangle$ exposed to a unitary transformation generated by the Hermitian operator \hat{O} can be quantified with the Quantum Fisher Information (QFI) and is related to its variance, i.e., $\text{QFI} = 4(\langle \psi | \hat{O}^2 | \psi \rangle - \langle \psi | \hat{O} | \psi \rangle^2)$ [36]. The Kitten states $|\chi_S^\pm(m)\rangle$ have QFIs equal to $4m^2$, with respect to the generator \hat{S}_y . Note that for the small Kitten states that is not the optimal choice for the QFI (\hat{S}_x or \hat{S}_z are better generators). This is shown in FIG. 4, where we plot the QFI with respect to all linear combinations of \hat{S}_x , \hat{S}_y and \hat{S}_z . This can also be seen by imagining tracing orthodromes/great circles on the Wigner functions in FIG. 1 and looking for the one that cuts through the sharpest/deepest interference fringes (the corresponding generator will be orthogonal to the plane spanned by the great circle). For

the small Kitten state, for example, the interference pattern along the equator is very coarse but along the meridian almost as fine as for the Dicke state. Compared to $|S, 0\rangle_x$ with $\text{QFI} = 2S^2 + 2S$ (with respect to \hat{S}_z, \hat{S}_y) we can define a lower threshold for the magnetic quantum number m_{crit} beyond which the QFI is larger than that of $|S, 0\rangle_x$, i.e.,

$$m_{\text{crit}} = \sqrt{\frac{S(S+1)}{2}} \approx \frac{S}{\sqrt{2}}. \quad (20)$$

The probability of an improvement in QFI is therefore the cumulative probability of all entangled-state cycles above that threshold (highlighted region in FIG. 3)

$$P_{\text{crit}} = \sum_{m=\lceil m_{\text{crit}} \rceil}^S 2(d_{m,0}^S)^2 = \sum_{b=0}^{S-\lceil m_{\text{crit}} \rceil} 2(d_{S-b,0}^S)^2, \quad (21)$$

where $\lceil x \rceil$, $\lfloor x \rfloor$ are the ceiling and floor functions.

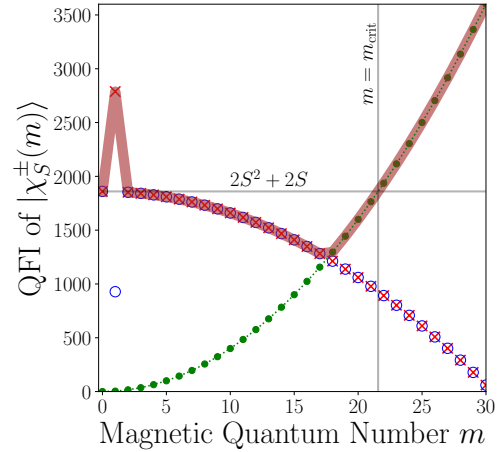


FIG. 4. QFI of the state $|\chi_S^\pm(m)\rangle$ with respect to the generators \hat{S}_x (blue circles), \hat{S}_y (green dots) and \hat{S}_z (red crosses) for $S = 30$. The broad brown curve shows the QFI with the optimal generator from all generators of the form $\sin \theta \cos \varphi \hat{S}_x + \sin \theta \sin \varphi \hat{S}_y + \cos \theta \hat{S}_z$. For $m = 0$ the state is just $|S, 0\rangle_y$.

FIG. 5 shows that P_{crit} becomes discontinuous when an additional magnetic quantum number m with non-zero population becomes larger than m_{crit} and starts contributing to P_{crit} (whenever $S - \lceil m_{\text{crit}} \rceil$ increases by two or equivalently $\lfloor (S - \lceil m_{\text{crit}} \rceil)/2 \rfloor$ by one, because only every second m has non-zero population). In the limit of large S , we can see that $\lfloor (S - \lceil m_{\text{crit}} \rceil)/2 \rfloor \xrightarrow{S \rightarrow \infty} \frac{\sqrt{2}-1}{2\sqrt{2}} S \approx S/6.82$, which means that the r -th jump happens when the spin becomes equal to $S_r = 1 + \frac{2\sqrt{2}}{\sqrt{2}-1} r \approx 1 + 7r$ (this periodicity of 7 gets occasionally interrupted by a segment of length 6, see FIG. 5 between the sixth and seventh jump). This means we can express P_{crit} piecewise on the segment $S \in [S_r, S_{r+1})$ as

$$P_{\text{crit}} = 2(d_{S,0}^S)^2 \alpha_r \approx \frac{2\alpha_r}{\sqrt{\pi S}}, \quad (22)$$

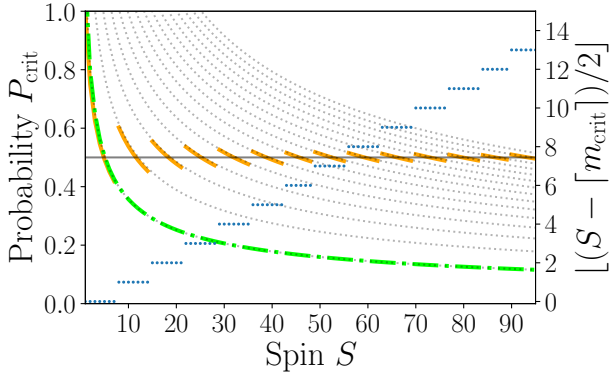


FIG. 5. Plot of the probability to increase the QFI P_{crit} (solid orange), its piecewise approximation $2\alpha_r/\sqrt{\pi S}$ (dotted gray), P_{cat} (dashdotted green). Note that, $P_{\text{cat}} = 2\alpha_0/\sqrt{\pi S}$. The other axis shows the number of non-zero population magnetic quantum number m that contribute to P_{crit} , i.e., $[(S - \lceil m_{\text{crit}} \rceil)/2]$ (blue dots).

where we defined the spin-dependent prefactors

$$\alpha_r(S) = \sum_{b=0}^r \left[\frac{d_{S-2b,0}^S}{d_{S,0}^S} \right]^2 \quad (23)$$

$$\approx 1 + \sum_{b=1}^r \sqrt{\frac{S}{\pi b(S-b)}} \frac{1 + \frac{1}{24b}}{(1 + \frac{1}{12b})^2}.$$

The spin dependence ends up being negligible over the segment they are defined on, meaning that any $S \in [S_r, S_{r+1})$ will yield roughly the same $\alpha_r(S)$. For a detailed explanation of this result, see Appendix A. Therein it is also shown that P_{crit} approaches 1/2 for large S which supports the numerical results in FIG. 5.

V. EXPERIMENTAL FEASIBILITY

The feasibility of this scheme in practice depends on two key factors: the ease of obtaining the initial state $|S, 0\rangle_x$ and how well the evolution can be shielded against noise.

A. The Initial State

The Dicke state $|S, 0\rangle$ possesses strong spin squeezing and has been studied extensively [37–43]. It should be noted that the initial state $|S, 0\rangle_x$ can also be generated from the same model in Eqs. (3-4) as was detailed in [25, 26]. For this, we start from the initial Dicke state $|S, S\rangle_z$ (easily achieved by pumping all spinors to their highest state) and set $\lambda_+ = \lambda_- = \lambda$, leading to the master equation $\dot{\hat{\rho}} = \Upsilon \mathcal{D}[\hat{S}_x]\hat{\rho}$. The system settling in $|S, 0\rangle_x$ (with probability $P \approx 1/\sqrt{\pi S}$), is heralded by the lack of any photoemissions and can therefore be postselected for. In [41], $|S, 0\rangle$ was theoretically generated with an efficiency of 15.5% and a fidelity of 99.52% for $N = 100$ spin 1/2 particles. In [40], these states are experimentally generated deterministically in ensembles of more than 10^4 spin-1 particles, but the final state is a superposition of Dicke

states with lower total spin, i.e., $\sum_{S'} |S', 0\rangle$. This would not significantly decrease the resulting QFI, as long as the distribution of S' 's is not too broad. The reported distributions are quite narrow with ranges of $0.99S < S' < S$. If inserted into our scheme this would result in superposition of different entangled-state cycles [similar m (same if only one parity involved, most likely one parity will dominate over time) but different S'].

B. Single-particle Decoherence

We use a general model for single-particle decoherence effects by including dephasing, pumping and decay of the individual atoms in the spin basis, which can be described with the Lindbladians $\sum_n \left(\mathcal{D}[\hat{S}_z^{(n)}/2]\hat{\rho} + \mathcal{D}[\hat{S}_+^{(n)}]\hat{\rho} + \mathcal{D}[\hat{S}_-^{(n)}]\hat{\rho} \right) \gamma_{\text{eff}}/2$, where for simulation purposes we assume all effects to be of equal strength γ_{eff} and the individual spinors to be of spin 1/2, i.e., $S_i^{(n)}$ to be the Pauli matrices. We simulate these single-particle effects using the permutational quantum invariant solver (PIQS) [44]. FIG. 6 shows the population of the different Kitten states over time under the influence of large collective and small single-particle decoherence. The moment an entangled-state cycle is reached in a single trajectory corresponds to reaching the steady state of the collective decay in the ensemble picture, i.e., when the population of the odd and even Kitten states with identical m become equal. The timescale for this process is governed by the decay of the smallest Kitten state, which is given by $1/\Upsilon$. After that, we are entering the time scale of the single-particle noise $1/(\gamma_{\text{eff}}N)$, which depopulates the Kitten states. To be able to prepare our desired state before noise gets the better of it, we need $\Upsilon > \gamma_{\text{eff}}N$.

One physical example for such processes could be the spontaneous emission from off-resonant excitation. For example, in the spin-1 implementation in ^{87}Rb using the D_1 -line [26, 30], this means that $\Upsilon \simeq (2n+1)g^2\Omega^2/(72\kappa\Delta^2)$ has to be larger than the effective decay rate from spontaneous emission given by $\gamma_{\text{eff}} \simeq \gamma\Omega^2/(12\Delta^2)$, where g is the atom-cavity coupling, Ω is the Rabi frequency of the laser, Δ is the detuning between atom and laser/cavity and γ is the natural line width of the $5^2P_{1/2}$ manifold. For $n = 0$, the ratio of these rates is $\gamma_{\text{eff}}N/\Upsilon \simeq 12N/C$, where $C = 2g^2/(\kappa\gamma)$ is the single-atom cooperativity. If we considered $\gamma_{\text{eff}}N/\Upsilon = 5 \times 10^{-2}$, it would require $C = 240N$, which will be hard to achieve for large atomic ensembles. This requirement can be relaxed by a factor $2n+1$ if the cavity is thermally populated.

In principle, the idea can be experimentally implemented in an engineered Dicke model, especially cavity QED implementations seem suitable [13, 45] due to being able to monitor the cavity output. Depending on the atomic species, the spontaneous emission rates of alkaline atoms are typically of the order of $\gamma = 3\text{--}6$ MHz. The experimental cavity parameters of current Dicke models [13, 45] have cooperativities below $C = 10$, which would require very large n . Modern

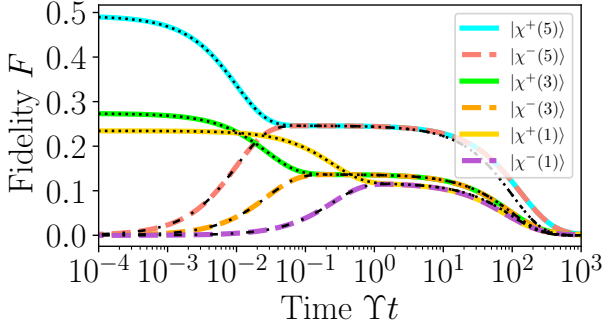


FIG. 6. Simulations of single-particle noise using permutational invariance starting from $|S, 0\rangle_x$. We plot the fidelity

$F = \left(\text{Tr} \sqrt{\sqrt{\hat{\rho}(t)} |\chi^\pm(m)\rangle \langle \chi^\pm(m)| \sqrt{\hat{\rho}(t)}} \right)^2$ of the quantum state during the evolution with the even (colored solid lines) and odd Kitten states (colored dashed lines) and the analytical fits $(d_{m,0}^S)^2 \exp(-\gamma_{\text{eff}} N t) [1 - \exp(-4\Gamma m^2 t)]$ (black dashdotted line) and $(d_{m,0}^S)^2 [\exp(-\gamma_{\text{eff}} N t) + \exp(-4\Gamma m^2 t)]$ (black dotted line). The parameters are $S = 5, N = 10$ and $\gamma_{\text{eff}}/\Upsilon = 0.001$.

micro- and nanocavity experiments can reach cooperativities beyond $C = 100$ [46–53], so that setups with $N \approx n$ are imaginable, but n is typically small.

It is therefore desirable to drastically increase the thermal population of the cavity. Doing that by increasing the temperature would require unrealistically high temperatures because of the large optical frequency and would also amplify spontaneous emission or other decoherence processes. A monochromatic thermal drive whose frequency matches that of the cavity as an input field could circumvent this issue. This could be achieved by sending black-body radiation through a monochromator or by using acousto-optical modulation of the output of a superluminescent diode [54]. Considering a two-sided cavity that interacts on one side with this hot reservoir (in) and on the other side with a reservoir in the vacuum state (out) would replace the current Lindblad-form with $\kappa_{\text{out}} \mathcal{D}[\hat{a}] + \kappa_{\text{in}}(n_{\text{th}} + 1) \mathcal{D}[\hat{a}] \hat{\rho} + \kappa_{\text{in}} n_{\text{th}} \mathcal{D}[\hat{a}^\dagger] \hat{\rho}$. Here, κ_{in} is derived from the cavity-reservoir coupling on the input side and κ_{out} on the other side. The resulting thermal cavity population would be $n = \kappa_{\text{in}} n_{\text{th}} / (\kappa_{\text{in}} + \kappa_{\text{out}})$, where n_{th} is the population of the input thermal reservoir [55]. This would change the collective decay to $\Upsilon = 2\lambda^2(2n+1)/[S(\kappa_{\text{in}} + \kappa_{\text{out}})]$.

Microwave-implementations of the engineered Dicke model have also been considered in [56], for example in fluxonium coupled to superconducting microwave cavities (frequencies of several GHz), the situation is similar with cooperativities $C > 100$ [57, 58], and n is naturally bigger.

Some states with weak multi-qubit entanglement end up being more robust against white noise than state with strong multi-qubit entanglement like GHZ states [35, 59]. Let us assume that we have such an admixture of our Kitten state (again for $N = 2S$ spin $1/2$ -spinors)

$$\hat{\rho}_{2S} = p |\chi_S^\pm(m)\rangle \langle \chi_S^\pm(m)| + (1-p) \mathbb{I}_{2S} / 2^{2S}. \quad (24)$$

If $2S - 2$ of the parties sharing the state locally measure $\hat{\sigma}_y$ and the result is that $S+m-1$ parties measure 0 and $S-m-1$ parties measure 1 (or vice versa), then the resulting state for the two remaining parties is

$$\hat{\rho}_2 = \frac{1}{1 + \frac{(1-p)\binom{2S}{S-m}}{2^{2S-2p}}} |\Psi^+\rangle \langle \Psi^+| + \frac{1}{1 + \frac{2^{2S-2p}}{(1-p)\binom{2S}{S-m}}} \mathbb{I}_2 / 4, \quad (25)$$

where $|\Psi^+\rangle = (|01\rangle + |10\rangle)/\sqrt{2}$. $\hat{\rho}_2$ doesn't adhere to local realism if $[1 + (1-p)\binom{2S}{S-m}/(2^{2S-2p})]^{-1} > 1/\sqrt{2}$. As this cannot arise from local operations on states adhering to local realism, $\hat{\rho}_{2S}$ must violate local realism if p exceeds the critical probability

$$p_{\text{crit}}^{\text{Kitten}} = \frac{\binom{2S}{S-m}}{\binom{2S}{S-m} + (\sqrt{2} - 1)2^{2S-2}}, \quad (26)$$

which increase with decreasing m leading to the Kitten states always being more robust than our initial state. This result is slightly larger than the critical value of Dicke states from [59] due to being a superposition of two Dicke states. We find that the critical value for the magnetic quantum number of the Kitten state for which the Kitten state becomes more robust than a GHZ state ($p_{\text{crit}}^{\text{GHZ}} = 2^{(1-2S)/2}$) roughly scales linearly with the spin ($[(S-m)/2S]_{\text{crit}} \approx 0.22$).

VI. CONCLUSIONS

We have shown that choosing Dicke states from a basis orthogonal to the dynamics as an initial state to dissipative one-axis twisting allows for the generation of large Kitten states. By choosing the eigenstate with magnetic quantum number zero we get a specific superposition that is biased towards the large magnetic quantum numbers and has been experimentally generated with satisfying fidelity in the past.

We have shown how the resulting Kitten states can have improved characteristics when it comes to quantum metrology or quantum secret sharing. The success can be monitored via the cavity output and we can post-select for it, however, even if in case of a failure the loss in QFI is likely not very big because all Kitten states are metrologically relevant.

Finally, we want to remark that the scheme could technically also be applied to the other Dicke states $|S, m\rangle_x$ with $0 < m < S$. In that case, we have an initial QFI $= 2S^2 + 2S - 2m^2$ resulting in $m_{\text{crit}} = \sqrt{[S(S+1) - m^2]/2}$. Compared to the initial state $|S, 0\rangle_x$, m_{crit} is lower for Dicke states with $m > 0$. The probability of increasing the QFI P_{crit} can then also be greater for some of the intermediate Dicke states. However, the average magnetic quantum number $\langle |m| \rangle$ and P_{Cat} are still the largest for $|S, 0\rangle_x$, so the resulting Kitten states and QFI are still going to be larger on average for $|S, 0\rangle_x$. It should be noted that the average resulting QFI will be the largest for the spin-coherent state because then the production of a small Kitten state with QFI close to $2S^2 + 2S$ is guaranteed. For half-integer spins, since $|S, 0\rangle$ does not exist, one can simply take $|S, \pm \frac{1}{2}\rangle$, which yields similarly biased distributions.

Other schemes that generate spin Cat states that are mainly based on the evolution with a one-axis twisting Hamiltonian. Our scheme's dissipative nature gives it the potential to operate at much faster time scales thanks to the thermal drive which can be beneficial in systems with limited coherence time. Our scheme settles in its entangled-state in a time $1/\Upsilon \geq 72\kappa\Delta^2/(2g^2) \approx 2 \mu\text{s}$ based on the realistic parameter set $\{\kappa, \Delta, g, \Omega\}/2\pi = \{0.05, 25, 0.25, 4\}$ GHz [26, 50]. Current experiments have time scales of the order of ms [60] or tenths of μs [7], which could be overcome with the additional factor $2n + 1$. It also does not require precise temporal control of the sys-

tem parameters besides keeping the electromagnetic fields constant unlike schemes based on machine optimization [61].

ACKNOWLEDGMENTS

This work makes use of the Quantum Toolbox in Python (QuTiP) [62, 63]. We thank Scott Parkins, Carlos Sánchez Muñoz and Sandro Wimberger for helpful discussions and comments.

-
- [1] E. Schrödinger, *Naturwissenschaften* **23**, 807 (1935).
 - [2] L. Pezzè, A. Smerzi, M. K. Oberthaler, R. Schmied, and P. Treutlein, *Reviews of Modern Physics* **90**, 035005 (2018).
 - [3] M. Hillery, V. Bužek, and A. Berthiaume, *Physical Review A* **59**, 1829 (1999).
 - [4] D. V. Sychev, A. E. Ulanov, A. A. Pushkina, M. W. Richards, I. A. Fedorov, and A. I. Lvovsky, *Nature Photonics* **11**, 379 (2017).
 - [5] A. Ourjoumtsev, H. Jeong, R. Tualle-Brouri, and P. Grangier, *Nature* **448**, 784 (2007).
 - [6] A. Facon, E.-K. Dietsche, D. Grosso, S. Haroche, J.-M. Raimond, M. Brune, and S. Gleyzes, *Nature* **535**, 262 (2016).
 - [7] T. Chalopin, C. Bouazza, A. Evrard, V. Makhalov, D. Dreon, J. Dalibard, L. A. Sidorenkov, and S. Nascimbene, *Nature Communications* **9**, 4955 (2018).
 - [8] B. Vlastakis, G. Kirchmair, Z. Leghtas, S. E. Nigg, L. Frunzio, S. M. Girvin, M. Mirrahimi, M. H. Devoret, and R. J. Schoelkopf, *Science* **342**, 607 (2013).
 - [9] C. Monroe, D. M. Meekhof, B. E. King, and D. J. Wineland, *Science* **272**, 1131 (1996).
 - [10] J. R. Friedman, V. Patel, W. Chen, S. K. Tolpygo, and J. E. Lukens, *Nature* **406**, 43 (2000).
 - [11] S. Glancy and H. M. de Vasconcelos, *JOSA B* **25**, 712 (2008).
 - [12] Y. M. Zhang, X. W. Li, W. Yang, and G. R. Jin, *Physical Review A* **88**, 043832 (2013).
 - [13] Z. Zhiqiang, C. H. Lee, R. Kumar, K. J. Arnold, S. J. Masson, A. S. Parkins, and M. D. Barrett, *Optica* **4**, 424 (2017).
 - [14] I. Aedo and L. Lamata, *Physical Review A* **97**, 042317 (2018).
 - [15] A. Safavi-Naini, R. J. Lewis-Swan, J. G. Bohnet, M. Gärttner, K. A. Gilmore, J. E. Jordan, J. Cohn, J. K. Freericks, A. M. Rey, and J. J. Bollinger, *Physical Review Letters* **121**, 040503 (2018).
 - [16] K. Baumann, C. Guerlin, F. Brennecke, and T. Esslinger, *Nature* **464**, 1301 (2010).
 - [17] K. Baumann, R. Mottl, F. Brennecke, and T. Esslinger, *Physical Review Letters* **107**, 140402 (2011).
 - [18] F. Verstraete, M. M. Wolf, and J. Ignacio Cirac, *Nature Physics* **5**, 633 (2009).
 - [19] H. Wetter, M. Fleischhauer, S. Linden, and J. Schmitt, *Physical Review Letters* **131**, 083801 (2023).
 - [20] D. Witthaut, F. Trimborn, and S. Wimberger, *Physical Review Letters* **101**, 200402 (2008).
 - [21] C. Marr, A. Beige, and G. Rempe, *Physical Review A* **68**, 033817 (2003).
 - [22] B. Kraus, H. P. Büchler, S. Diehl, A. Kantian, A. Micheli, and P. Zoller, *Physical Review A* **78**, 042307 (2008).
 - [23] S. Diehl, A. Micheli, A. Kantian, B. Kraus, H. P. Büchler, and P. Zoller, *Nature Physics* **4**, 878 (2008).
 - [24] E. G. Dalla Torre, J. Otterbach, E. Demler, V. Vuletic, and M. D. Lukin, *Physical Review Letters* **110**, 120402 (2013).
 - [25] A. Chia and A. S. Parkins, *Physical Review A* **77**, 033810 (2008).
 - [26] C. Groiseau, *Cavity QED with Multilevel Atoms: Generation of Nonclassical States*, Ph.D. thesis, ResearchSpace@ Auckland (2021).
 - [27] C. Sánchez Muñoz, B. Buča, J. Tindall, A. González-Tudela, D. Jaksch, and D. Porras, *Physical Review A* **100**, 042113 (2019).
 - [28] G. S. Agarwal, *Physical Review A* **24**, 2889 (1981).
 - [29] H.-P. Breuer and F. Petruccione, *The Theory of Open Quantum Systems* (Oxford University Press, 2002).
 - [30] S. J. Masson, M. D. Barrett, and S. Parkins, *Physical Review Letters* **119**, 213601 (2017).
 - [31] F. Dimer, B. Estienne, A. S. Parkins, and H. J. Carmichael, *Physical Review A* **75**, 013804 (2007).
 - [32] J. J. Sakurai and J. Napolitano, *Modern Quantum Mechanics* (2020).
 - [33] H. Carmichael, *An Open Systems Approach to Quantum Optics: Lectures Presented at the Université Libre de Bruxelles October 28 to November 4, 1991*, edited by H. Araki, E. Brézin, J. Ehlers, U. Frisch, K. Hepp, R. L. Jaffe, R. Kippenhahn, H. A. Weidenmüller, J. Wess, J. Zittartz, and W. Beiglböck, *Lecture Notes in Physics Monographs*, Vol. 18 (Springer, Berlin, Heidelberg, 1993).
 - [34] C. Groiseau, S. J. Masson, and S. Parkins, *Physical Review A* **104**, 053721 (2021).
 - [35] A. Sen(De), U. Sen, and M. Żukowski, *Physical Review A* **68**, 032309 (2003).
 - [36] S. L. Braunstein and C. M. Caves, *Physical Review Letters* **72**, 3439 (1994).
 - [37] S. Raghavan, H. Pu, P. Meystre, and N. P. Bigelow, *Optics Communications* **188**, 149 (2001).
 - [38] X.-Y. Luo, Y.-Q. Zou, L.-N. Wu, Q. Liu, M.-F. Han, M. K. Tey, and L. You, *Science* **355**, 620 (2017).
 - [39] C. Thiel, J. von Zanthier, T. Bastin, E. Solano, and G. S. Agarwal, *Physical Review Letters* **99**, 193602 (2007).
 - [40] Y.-Q. Zou, L.-N. Wu, Q. Liu, X.-Y. Luo, S.-F. Guo, J.-H. Cao, M. K. Tey, and L. You, *Proceedings of the National Academy of Sciences* **115**, 6381 (2018).
 - [41] S. J. Masson and S. Parkins, *Physical Review A* **99**,

- 023822 (2019).
- [42] J. K. Stockton, R. van Handel, and H. Mabuchi, *Physical Review A* **70**, 022106 (2004).
 - [43] B. Lücke, J. Peise, G. Vitagliano, J. Arlt, L. Santos, G. Tóth, and C. Klempt, *Physical Review Letters* **112**, 155304 (2014).
 - [44] N. Shammah, S. Ahmed, N. Lambert, S. De Liberato, and F. Nori, *Physical Review A* **98**, 063815 (2018).
 - [45] E. J. Davis, G. Bentsen, L. Homeier, T. Li, and M. H. Schleier-Smith, *Physical Review Letters* **122**, 010405 (2019).
 - [46] C. Sames, H. Chibani, C. Hamsen, P. A. Altin, T. Wilk, and G. Rempe, *Physical Review Letters* **112**, 043601 (2014).
 - [47] R. Reimann, W. Alt, T. Kampschulte, T. Macha, L. Ratschbacher, N. Thau, S. Yoon, and D. Meschede, *Physical Review Letters* **114**, 023601 (2015).
 - [48] F. Haas, J. Volz, R. Gehr, J. Reichel, and J. Estève, *Science* **344**, 180 (2014).
 - [49] R. Gehr, J. Volz, G. Dubois, T. Steinmetz, Y. Colombe, B. L. Lev, R. Long, J. Estève, and J. Reichel, *Physical Review Letters* **104**, 203602 (2010).
 - [50] G. Barontini, L. Hohmann, F. Haas, J. Estève, and J. Reichel, *Science* **349**, 1317 (2015).
 - [51] J. D. Thompson, T. G. Tiecke, N. P. de Leon, J. Feist, A. V. Akimov, M. Gullans, A. S. Zibrov, V. Vuletić, and M. D. Lukin, *Science* **340**, 1202 (2013).
 - [52] T. G. Tiecke, J. D. Thompson, N. P. de Leon, L. R. Liu, V. Vuletić, and M. D. Lukin, *Nature* **508**, 241 (2014).
 - [53] P. Samutpraphoot, T. \DJor\djević, P. L. Ocola, H. Bernien, C. Senko, V. Vuletić, and M. D. Lukin, *Physical Review Letters* **124**, 063602 (2020).
 - [54] I. Straka, J. Mika, and M. Ježek, *Optics Express* **26**, 8998 (2018).
 - [55] G. Hennin Arencibia, *Catching Quantum Jumps Through Monitored Thermal Light*, Thesis, ResearchSpace@Auckland (2023).
 - [56] A. L. Grimsmo, *Controlling the Quantum State of Light and Matter with Cavity QED*, Doctoral Thesis, NTNU (2014).
 - [57] N. Earnest, S. Chakram, Y. Lu, N. Irons, R. K. Naik, N. Leung, L. Ocola, D. A. Czaplewski, B. Baker, J. Lawrence, J. Koch, and D. I. Schuster, *Physical Review Letters* **120**, 150504 (2018).
 - [58] Y.-H. Lin, L. B. Nguyen, N. Grabon, J. San Miguel, N. Pankratova, and V. E. Manucharyan, *Physical Review Letters* **120**, 150503 (2018).
 - [59] W. Laskowski, T. Vertesi, and M. Wiesniak, arXiv preprint arXiv:1412.8745 (2014), arXiv:1412.8745.
 - [60] Y. A. Yang, W.-T. Luo, J.-L. Zhang, S.-Z. Wang, C.-L. Zou, T. Xia, and Z.-T. Lu, *Nature Photonics* **19**, 89 (2025).
 - [61] J. Huang, H. Huo, M. Zhuang, and C. Lee, *Physical Review A* **105**, 062456 (2022).
 - [62] J. R. Johansson, P. D. Nation, and F. Nori, *Computer Physics Communications* **183**, 1760 (2012).
 - [63] J. R. Johansson, P. D. Nation, and F. Nori, *Computer Physics Communications* **184**, 1234 (2013).
 - [64] M. Abramowitz and I. A. Stegun, *Handbook of Mathematical Functions with Formulas, Graphs, and Mathematical Tables* (U.S. Government Printing Office, 1948).

Appendix A: Calculations

We can reformulate the spherical harmonics as

$$\begin{aligned} Y_{S-2b}^S(-\frac{\pi}{2}, 0) &= (-1)^{S-2b} \sqrt{\frac{(2S+1)(2b)!}{4\pi(2S-2b)!}} P_{S-2b}^S(0) \\ &= (-1)^{S-2b} \frac{\sqrt{2S+1} \sqrt{\Gamma(2b+1)} {}_2F_1(-S, S+1, -S+2b+1, \frac{1}{2})}{\sqrt{4\pi} \Gamma(1-S+2b) \sqrt{\Gamma(2S-2b+1)}}, \end{aligned} \quad (\text{A1})$$

where P is the associated Legendre polynomial and ${}_2F_1$ the hypergeometric function [64], which we can express in terms of Γ -functions

$${}_2F_1(-S, S+1, -S+2b+1, \frac{1}{2}) = \frac{2^{S-2b} \Gamma(1-S+2b)}{\Gamma(\frac{1}{2}-S+b) \Gamma(b+1)}. \quad (\text{A2})$$

This allows us to compute the coefficients

$$\begin{aligned} \alpha_r(S) &= \sum_{b=0}^r \left[\frac{d_{S-2b,0}^S}{d_{S,0}^S} \right]^2 \\ &= \sum_{b=0}^r \left[\frac{Y_{S-2b}^S(-\frac{\pi}{2}, 0)}{Y_S^S(-\frac{\pi}{2}, 0)} \right]^2 \\ &= \sum_{b=0}^r \left[\frac{\sqrt{\Gamma(2b+1)} \Gamma(\frac{1}{2}-S) \sqrt{\Gamma(2S+1)}}{\sqrt{\Gamma(2S-2b+1)} \Gamma(b+1) \Gamma(\frac{1}{2}+b-S) 2^{2b}} \right]^2 \\ &\approx 1 + \sum_{b=1}^r \sqrt{\frac{S}{\pi b(S-b)}} \frac{1 + \frac{1}{24b}}{(1 + \frac{1}{12b})^2}, \end{aligned} \quad (\text{A3})$$

where, in the third step we used that for non-negative integers j , $\Gamma(\frac{1}{2}-j) = (-4)^j j! \sqrt{\pi} / [(2j)!]$ [64] and the Stirling approximation [we include an additional order for the terms solely depending on the potentially small b , i.e., $b! \approx b^b e^{-b} \sqrt{2\pi b} (1 + \frac{1}{12b})$] [64].

Since the function in the series is integrable and decreasing monotonically for positive b , we can estimate a lower bound with the definite integral

$$\alpha_r(S) \geq 1 + \int_1^{r+1} db \sqrt{\frac{S}{\pi b(S-b)}} \frac{1 + \frac{1}{24b}}{(1 + \frac{1}{12b})^2}, \quad (\text{A4})$$

which we can then use to estimate the critical probability in the limit of large spin, i.e.,

$$\begin{aligned} P_{\text{crit}} &\geq \frac{2[1 + \int_1^{\lfloor (S - \lceil m_{\text{crit}} \rceil)/2 \rfloor + 1} db \sqrt{\frac{S}{\pi b(S-b)}} \frac{1 + \frac{1}{24b}}{(1 + \frac{1}{12b})^2}]}{\sqrt{\pi S}} \\ &= \frac{2[1 + \int_1^{\lfloor (S - \lceil m_{\text{crit}} \rceil)/2 \rfloor + 1} db \sqrt{\frac{S}{\pi b(S-b)}} (1 + \mathcal{O}(\frac{1}{b}))]}{\sqrt{\pi S}} \\ &= 2[\frac{1}{\sqrt{\pi S}} + \frac{2}{\pi} \arctan \sqrt{\frac{b}{S-b}}]_1^{\lfloor \frac{S - \lceil m_{\text{crit}} \rceil}{2} \rfloor + 1} + \mathcal{O}(S^{-\frac{1}{2}})] \\ &\xrightarrow{S \rightarrow \infty} \frac{4}{\pi} \arctan \sqrt{\frac{\sqrt{2}-1}{\sqrt{2}+1}} \\ &= \frac{1}{2}. \end{aligned} \quad (\text{A5})$$

This can be generalized to the case, where we demand that the resulting QFI has to be larger than fS^2 ($m_{\text{crit}} = fS^2$) with $f \in [0, 4]$, i.e.,

$$P_{\text{crit}}(f) = \frac{4}{\pi} \arctan \sqrt{\frac{2 - \sqrt{f}}{2 + \sqrt{f}}}, \quad (\text{A6})$$

which is depicted in FIG. 7.

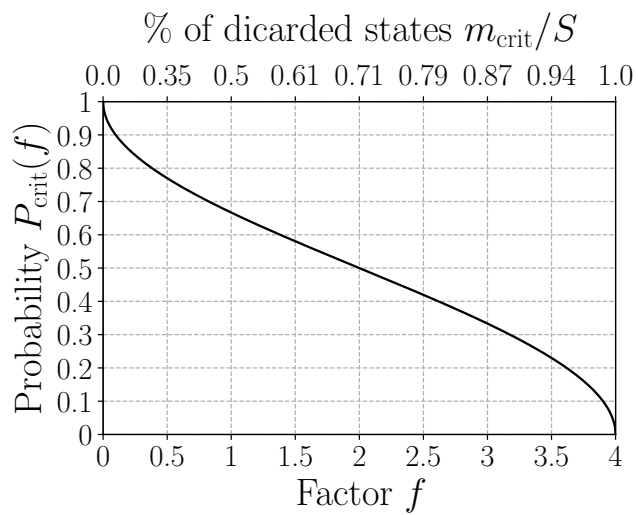


FIG. 7. Plot of the probability $P_{\text{crit}}(f)$ to overcome a QFI of fS^2 against f in the limit of infinite S . We also show what a given f means in terms of the ratio of Kitten states that have to be overcome $m_{\text{crit}}/S = \sqrt{f}/2$.